PNAS RESEARCH ARTICLE | IMMUNOLOGY AND INFLAMMATION

Essential requirement for IER3IP1 in B cell development

Xue Zhong[a], James J. Moresco[a], Katie Keller[a], Danielle Renee Lazaro[a], Claire Ely[a], Eva Marie Y. Moresco[a], Bruce Beutler[a,1], and Jin Huk Choi[a,b,1]

Contributed by Bruce Beutler; received July 26, 2023; accepted October 5, 2023; reviewed by Jean-Laurent Casanova and Christopher C. Goodnow

In a forward genetic screen of mice with *N*-ethyl-*N*-nitrosourea-induced mutations for aberrant immune function, we identified animals with low percentages of B220$^+$ cells in the peripheral blood. The causative mutation was in *Ier3ip1*, encoding immediate early response 3 interacting protein 1 (IER3IP1), an endoplasmic reticulum membrane protein mutated in an autosomal recessive neurodevelopmental disorder termed Microcephaly with simplified gyration, Epilepsy and permanent neonatal Diabetes Syndrome (MEDS) in humans. However, no immune function for IER3IP1 had previously been reported. The viable hypomorphic *Ier3ip1* allele uncovered in this study, identical to a reported *IER3IP1* variant in a MEDS patient, reveals an essential hematopoietic-intrinsic role for IER3IP1 in B cell development and function. We show that IER3IP1 forms a complex with the Golgi transmembrane protein 167A and limits activation of the unfolded protein response mediated by inositol-requiring enzyme-1α and X-box binding protein 1 in B cells. Our findings suggest that B cell deficiency may be a feature of MEDS.

IER3IP1 | B cells | unfolded protein response | TMEM167A | ENU

B cell development is a highly regulated process whereby functional peripheral subsets are produced from hematopoietic stem cells in the bone marrow (BM) (1). During development, B cells express numerous cell surface proteins, such as immunoglobulins, following a characteristic pattern and timing. Upon activation by antigen, mature naive B cells differentiate into plasma cells engaging in high-level immunoglobulin secretion which requires expansion of the secretory pathway (2, 3). Thus, B cell development and function are heavily dependent on the endoplasmic reticulum (ER), which manages the folding of nascent integral membrane proteins and proteins destined for secretion (4). Conditions that lead to the accumulation of unfolded proteins in the ER trigger ER stress, also known as the unfolded protein response (UPR). The UPR consists of the coordinated activities of one or more signaling pathways that attempt to resolve unfolded proteins using chaperones for refolding, proteasome-mediated degradation, and downregulation of translation. Elevated or prolonged UPR signaling may trigger apoptosis.

Immediate early response 3 interacting protein 1 (IER3IP1) is a small ER membrane protein reported to function as an attenuator of the UPR (5–7). IER3IP1 is expressed in multiple tissues including brain, pancreas, heart, muscle, kidney, lung, and immune cells (8). While many pathological effects of *IER3IP1* mutations in MEDS (Microcephaly with simplified gyration, Epilepsy and permanent neonatal Diabetes Syndrome) have been studied (9–13).

In this study, we identified two recessive ENU (*N*-ethyl-*N*-nitrosourea)-induced missense mutations in *Ier3ip1*, each causing severe impairment of B lymphopoiesis in mice. Reduced proliferation, immunoglobulin class switching, cell cycle progression, and cytosolic Ca^{2+} flux, and increased ER stress were detected in the splenic B cells of homozygotes. Through mass spectrometry (MS)–based IER3IP1 interactome analysis, we identified a small Golgi apparatus membrane protein, TMEM167A, as a putative interactor with IER3IP1, and demonstrated that expression of TMEM167A is dependent upon expression of IER3IP1.

Results

Identification of *Ier3ip1* Mutations Responsible for B Cell Deficiency in Mice. We conducted a forward genetic screen of ENU-mutagenized mice to identify genes involved in immune cell development and function, using flow cytometric analysis of peripheral blood to detect abnormal phenotypes as described previously (14–16). We identified several third-generation (G3) mice descended from two independent G1 male founders with low percentages of B220$^+$ cells in the peripheral blood (Fig. 1*A*). The phenotypes, which we named *alarmist* and *emergent*, were transmitted as recessive traits. By automated meiotic mapping (17, 18), the two phenotypes were correlated with nonidentical allelic

Significance

In 2011, mutations in the human gene *IER3IP1* (immediate early response 3 interacting protein 1) were reported to cause the neurodevelopmental disorder MEDS (Microcephaly with simplified gyration, Epilepsy and permanent neonatal Diabetes Syndrome). Whereas the neuronal pathology of MEDS has been well described, the requirement for IER3IP1 in immunity had escaped notice. Using a forward genetic screen in mice, we identified two viable missense mutations in *Ier3ip1*, one of which is identical to a reported IER3IP1 variant in a MEDS patient. We identified an essential role for IER3IP1 in B cell development and function. This mouse strain is a faithful model of human MEDS with B cell deficiency, useful for the study of IER3IP1 molecular functions and their physiological consequences.

Author affiliations: [a]Center for the Genetics of Host Defense, University of Texas Southwestern Medical Center, Dallas, TX 75390-8505; and [b]Department of Immunology, University of Texas Southwestern Medical Center, Dallas, TX 75390

Author contributions: X.Z., B.B., and J.H.C. designed research; X.Z., J.J.M., K.K., D.R.L., C.E., and J.H.C. performed research; X.Z., J.J.M., and J.H.C. analyzed data; and X.Z., E.M.Y.M., B.B., and J.H.C. wrote the paper.

Reviewers: J.-L.C., The Rockefeller University; and C.C.G., Garvan Institute of Medical Research.

The authors declare no competing interest.

[1]To whom correspondence may be addressed. Email: Bruce.Beutler@UTSouthwestern.edu or Jin.Choi@UTSouthwestern.edu.

This article contains supporting information online at https://www.pnas.org/lookup/suppl/doi:10.1073/pnas.2312810120/-/DCSupplemental.

Published November 7, 2023.

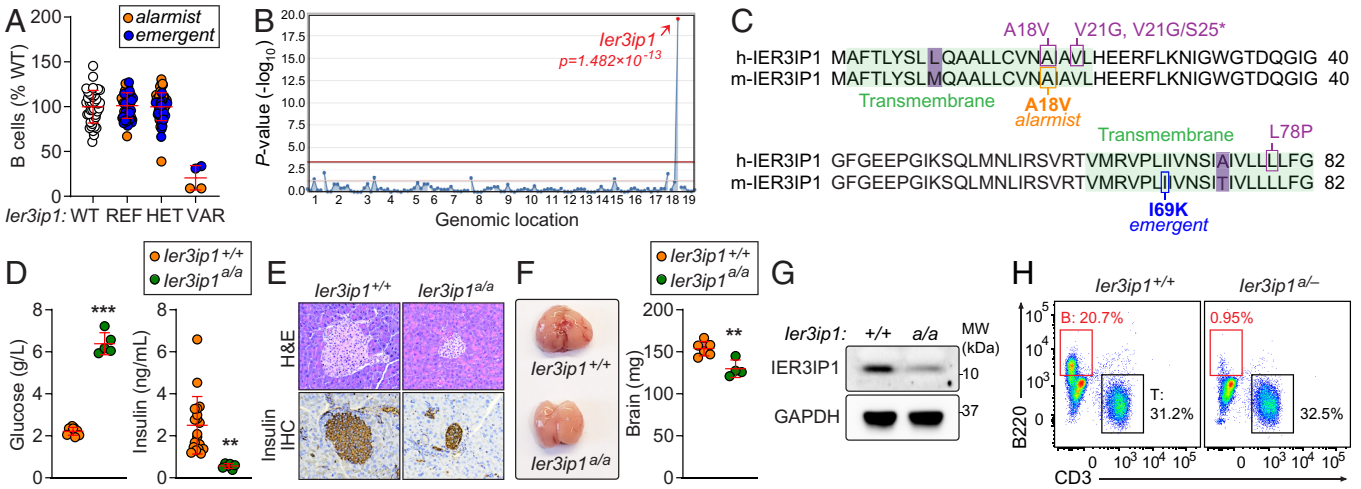

Fig. 1. Identification of mouse *Ier3ip1* mutations responsible for B cell deficiency. (*A*) The frequency of peripheral blood B cells from third-generation (G3) descendants of two independent ENU-mutagenized male mice (G1), with REF (+/+), HET (+/mutant), or VAR (mutant/mutant) genotypes for *Ier3ip1* (n = 2 to 43 mice/genotype). Data were normalized to the average B cell frequency of age-matched C57BL/6 mice at the time of the experiment (n = 20 mice/experiment). (*B*) Manhattan plot showing $-log_{10}$ *P*-values (*y* axis) plotted vs. the chromosomal positions of mutations (*x* axis) identified in the G1 founders of the affected pedigrees. The *alarmist* and *emergent* pedigrees were combined for linkage analysis (i.e., superpedigree mapping) (18). (*C*) Sequence alignment of human and mouse IER3IP1. Transmembrane domains are highlighted in green. Discordant amino acids between human and mouse IER3IP1 are highlighted in violet. The *alarmist* (A18V) and *emergent* (I69K) mutations identified by forward genetic screening in the present study are boxed in orange and blue, respectively. Natural *IER3IP1* variants reported to cause MEDS in humans are boxed in violet. (*D*) Serum glucose and insulin levels in 4-wk-old $Ier3ip1^{a/a}$ and wild-type littermates (n = 5 to 19 mice/genotype). (*E*) Representative hematoxylin and eosin (H&E) staining and insulin immunohistochemistry (IHC) of pancreases isolated from 8-wk-old $Ier3ip1^{a/a}$ and wild-type littermates. (*F*) A representative photograph and weights of brains isolated from 12-wk-old $Ier3ip1^{a/a}$ and wild-type littermates (n = 4 to 5 mice/genotype). (*G*) Immunoblot analysis of IER3IP1 and GAPDH in total cell lysates of splenic pan B cells isolated from $Ier3ip1^{a/a}$ and wild-type littermates. (*H*) Representative flow cytometry plots showing B and T cell frequencies in the peripheral blood from 8-wk-old $Ier3ip1^{a/-}$ and wild-type littermates. Data are representative of one (*A*) or three independent experiments (*D*–*H*). Data points represent individual mice (*A*, *D*, and *F*). Error bars indicate SD. *P* values were determined by one-way ANOVA with Dunnett's multiple comparisons (*A*) or Student's *t* test (*D* and *F*). $^{**}P < 0.01$; $^{***}P < 0.001$.

mutations in *Ier3ip1* with a composite *P* value of 3.9×10^{-20} (Fig. 1*B*). The encoded protein, IER3IP1, is an 82-amino acid ER-resident transmembrane protein.

The *alarmist* mutation resulted in an alanine (A) to valine (V) substitution at position 18 (A18V) in the first transmembrane domain of IER3IP1 (Fig. 1*C*), which was predicted to be damaging by PolyPhen-2 (score = 1.000) (19). The *emergent* mutation resulted in an isoleucine (I) to lysine (K) substitution at position 69 (I69K) in the second transmembrane domain of the protein (Fig. 1*C*). IER3IP1 orthologs from humans and mice share 97.56% amino acid sequence identity (Fig. 1*C*). Importantly, a homozygous variant of human *IER3IP1* resulting in MEDS and identical to the *alarmist* mutation was recently reported (12). Therefore, in the studies below, we chose to analyze the *alarmist* allele exclusively.

In addition to MEDS caused by *IER3IP1* variants in humans, rat insulin II promoter-cre driven IER3IP deletion in pancreatic β cells causes insulin-deficient diabetes in mice (6). We found that *alarmist* mice had significantly elevated fasting blood glucose levels together with lower serum insulin concentrations compared to wild-type littermates as early as 4 wk of age (Fig. 1*D*). Since IER3IP1 inhibition impairs β cell survival and proliferation (5), we performed histological analysis and found that pancreases from *alarmist* mice showed greatly reduced islet size compared to those from wild-type littermates (Fig. 1*E*). However, immunohistochemical analysis confirmed the expression of insulin in the pancreas of *alarmist* mice (Fig. 1*E*). This suggests that insulin-deficient diabetes results from a reduction in islet size and β cell mass in *alarmist* mice; however, it is possible that insulin secretion by the remaining viable β cells is also defective. Consistent with observations in a human patient with the homozygous *IER3IP1* A18V variant (12), the *alarmist* mutation (A18V) caused microcephaly in mice (Fig. 1*F*).

Next, we examined the effect of the *alarmist* mutation on protein stability. Decreased levels of IER3IP1 were detected in splenic B cells from *alarmist* mice ($Ier3ip1^{a/a}$) carrying the A18V mutation compared to those in B cells from wild-type littermates, suggesting that the *alarmist* mutation impairs protein stability (Fig. 1*G*).

According to publicly available data from the International Mouse Phenotyping Consortium (https://www.mousephenotype.org/data/genes/MGI:1913441), knockout of *Ier3ip1* causes embryonic lethality at E9.5 in mice. To verify causation, we crossed *alarmist* heterozygotes ($Ier3ip1^{a/+}$) with CRISPR/Cas9-targeted *Ier3ip1* heterozygotes ($Ier3ip1^{+/-}$), which were phenotypically normal in both cases, to generate *Ier3ip1* compound heterozygotes ($Ier3ip1^{a/-}$) with simple heterozygosity for all residual ENU-induced mutations. We found that offspring with the $Ier3ip1^{a/-}$ genotype were not born at expected Mendelian frequencies ($P = 0.0007$; χ^2 test; n = 45 mice: 20 $Ier3ip1^{+/+}$, 23 $Ier3ip1^{+/-}$ or $Ier3ip1^{a/+}$, 2 $Ier3ip1^{a/-}$). These results demonstrate that although compatible with life, compound heterozygosity for the *alarmist* and null alleles of *Ier3ip1* caused reduced viability. The *Ier3ip1* compound heterozygotes showed reduced frequencies of B cells in peripheral blood compared with WT littermates (Fig. 1*H*). This result established a causative relationship between the $Ier3ip1^{alarmist}$ mutation and the observed phenotype in $Ier3ip1^{a/-}$ mice. Together, these data demonstrate that alterations in glucose metabolism, brain development, and B cell development all result from a viable hypomorphic missense mutation (A18V) in *Ier3ip1* in mice.

Impaired B Cell Development Caused by *Ier3ip1* Mutation. We immunophenotyped mice by complete blood count testing and flow cytometry analysis of immune cells in blood, BM, thymus, spleen, and peritoneum. The *alarmist* mice had reduced numbers of white blood cells, lymphocytes, and monocytes; neutrophil numbers were normal (*SI Appendix*, Fig. S1 *A*–*D*). The mice also manifested mild anemia with significant macrocytosis and anisocytosis. Mean platelet volume and platelet count were also elevated (*SI Appendix*, Fig. S1 *E*–*M*). Gross examination

of lymphoid organs showed that the *alarmist* mice had smaller thymi compared to wild-type littermates (Fig. 2*A*; 45.2% reduction when determined by total thymocyte counts); spleens from *alarmist* mice appeared normal (Fig. 2*A*). The frequency of double-negative (DN) thymocytes was increased in *alarmist* mice compared to wild-type littermates. Within the DN compartment, the frequency of DN3 thymocytes was increased indicating a defect in thymocyte maturation in *alarmist* mice. The proportion of γ/δ- and β-TCR expressing DN thymocytes was not changed. The percentage of double-positive (DP) thymocytes was decreased; however, *alarmist* mice had normal frequencies of single-positive T cells in the thymus (Fig. 2*B*). We observed increased expression of the surface glycoprotein CD44 on CD8+ T cells in the peripheral blood of *alarmist* mice; these cells encompass recently activated, expanding, and memory phenotype cells (Fig. 2*C*). Overall, T cell development appeared largely normal in *alarmist* mice. Since the *alarmist* mutation primarily impairs B cells, the B cell–to–T cell ratio was decreased (Fig. 2*D*).

We examined the hematopoietic stem and progenitor cell (HSPC) populations in the BM. The *alarmist* mutation did not appreciably affect the total HSPC population, including long-term HSCs, short-term HSCs, multipotent progenitors, lymphoid-primed multipotential progenitors, common lymphoid progenitors, common myeloid progenitors (CMP), megakaryocyte–erythrocyte progenitors, or granulocyte-macrophage progenitors (Fig. 2*E*). These findings suggest that IER3IP1 functions in B cell development after hematopoietic lineage commitment.

The *alarmist* mice had reduced numbers of B cell progenitors in the BM beginning at the pre-pro-B stage (Fig. 2*F*) and very few cells progressed from the pre-B to the immature B stage (Fig. 2 *F* and *H*). In addition, the total numbers and frequencies of mature recirculating B cells in the BM were significantly decreased in *alarmist* mice compared to wild-type littermates (Fig. 2 *F* and *H*). In the spleen, we found that *alarmist* mice had reduced numbers of transitional B cells in all stages (Fig. 2*F*). The reduced proportions of T2 and T3 B cells with concomitant increased proportions of T1 B cells in spleens from *alarmist* mice compared to wild-type littermates indicate that the mutation also significantly impairs B cell maturation in the spleen (Fig. 2*I*). Consistent with the reduction in T2 B cells (Fig. 2 *F* and *I*), the total numbers and frequencies of follicular B cells, direct descendent of T2 B cells, were decreased in *alarmist* mice compared to wild-type littermates (Fig. 2 *F* and *L*). The frequencies of T2 to marginal zone precursors (Fig. 2*J*) and MZ B cells (Fig. 2 *K* and *L*) in the spleen appeared increased in *alarmist* mice compared to wild-type littermates, but the total numbers were decreased (Fig. 2*F*) as a result of decreased T2 B cells (Fig. 2 *F* and *I*). Although the phenotypic effect was not as robust as in B2 cells, the *alarmist* mutation also caused diminished numbers and altered frequencies of B1 cells and their subpopulations [Fig. 2 *F*, *M*, and *N*; (20)]. Consequently, significantly decreased basal levels of major immunoglobulin isotypes were detected in the serum of *alarmist* mice compared with wild-type littermates, with the exception of IgE and IgM (Fig. 2*O*). The *alarmist* mutation had no effect on serum IgE levels; however, serum IgM levels were elevated. Collectively, these data demonstrate that IER3IP1 is essential for B cell development after the lymphoid progenitor stage and at or before the pre-pro-B stage in the BM, and throughout development in the spleen.

Effect of *Ier3ip1* Mutation on B Cell Function and the UPR. To determine the cellular origin of the defect in B development, we reconstituted irradiated wild-type (CD45.1) or *alarmist* mice (*Ier3ip1*$^{a/a}$; CD45.2) with unmixed *Ier3ip1*$^{+/+}$ (CD45.2), *Ier3ip1*$^{a/a}$ (CD45.2), or wild-type (CD45.1) BM cells. The BM cells from *alarmist* donors were unable to repopulate B cells in wild-type recipients (CD45.1) whereas BM cells derived from wild-type donors (CD45.1) were able to fully reconstitute B cells in *alarmist* recipients (CD45.2; Fig. 3*A*). In addition, *alarmist* recipients reconstituted with wild-type (CD45.1) BM mounted T cell-dependent (TD) antibody responses to aluminum hydroxide-precipitated ovalbumin (OVA) comparable to those of irradiated wild-type (CD45.1) recipients engrafted with wild-type (*Ier3ip1*$^{+/+}$) BM (Fig. 3*C*). In contrast, irradiated wild-type (CD45.1) recipients engrafted with *alarmist* BM showed significantly decreased TD antibody responses (Fig. 3*C*). However, the BM chimeras with *Ier3ip1*$^{a/a}$ cells in either the hematopoietic or nonhematopoietic compartment mounted comparable T cell-independent antibody responses to (4-hydroxy-3-nitrophenyl) acetyl-Ficoll (NP-Ficoll) compared with wild-type recipients of wild-type BM (Fig. 3*D*). Furthermore, increased proportions of T cells, a reflection of altered B cell-to-T cell ratio, were also observed in the peripheral blood of irradiated wild-type (CD45.1) recipients engrafted with *alarmist* BM (Fig. 3*B*). These data indicate that the defects in B cell development and TD antibody responses result from reduced IER3IP1 function in the hematopoietic compartment, most likely in B cells themselves.

Next, B cell function was examined. LPS- and IL-4-induced class-switch recombination to IgG1 and cell division were significantly decreased in *Ier3ip1* mutant splenic B cells compared to wild-type cells (Fig. 3 *E*–*G*). Cell cycle analysis of naive *Ier3ip1* mutant B cells during LPS- and IL-4-induced activation showed a significant arrest in M phase compared to wild-type cells (Fig. 3 *H* and *I*). These results indicate that IER3IP1 is indispensable for B cell function.

Taking into account the ER and Golgi localization of IER3IP1 and its known function in limiting UPR in cerebral organoids and pancreatic β cells (7, 14), we hypothesized that IER3IP1 may serve a similar function in B cells. To test this, we examined the effect of the IER3IP1 mutation on UPR activation in unstimulated splenic B cells and after treatment with the ER stress inducer tunicamycin (Fig. 3*J*). The basal level of immunoglobulin heavy chain binding protein (BiP), which is proportional to the level of misfolded protein in the ER (21), and the level of inositol-requiring enzyme-1α (IRE1α), a proximal sensor for UPR that transmits the unfolded protein signal across the ER membrane (22), were increased in *Ier3ip1* mutant B cells compared to wild-type cells. The basal level of spliced XBP1 (XBP1s), a direct downstream target of IRE1α, was increased in unstimulated *Ier3ip1* mutant B cells compared to wild-type cells and was further elevated following ER stress induction. The levels of total and phosphorylated protein kinase-like ER kinase (PERK), an ER membrane resident protein that couples ER stress signals to translation inhibition through phosphorylation of eukaryotic initiation factor 2α [eIF2α; (23)], were slightly decreased. However, phosphorylation of eIF2 and levels of activating transcription factor 4 (ATF4) and C/EBP homologous protein (CHOP), downstream effectors of PERK upon ER stress induction, were comparable in *Ier3ip1* mutant B cells with respect to wild-type cells. We also observed increased basal levels of activating transcription factor 6 (ATF6), an ER membrane-anchored transcription factor activated by site-1 and -2 proteases, with concomitant increase in its cleaved form [blue arrowhead; (24)] upon ER stress induction in *Ier3ip1* mutant B cells compared with wild-type cells. However, ATF6 activation, as evidenced by the level of cleaved ATF6, was less robust than IRE1α activation leading to XBP1 splicing (XBP1s). These data suggest that the *Ier3ip1* mutation forces UPR activation in primary B cells at least through the IRE1α-XBP1 dependent signaling axis.

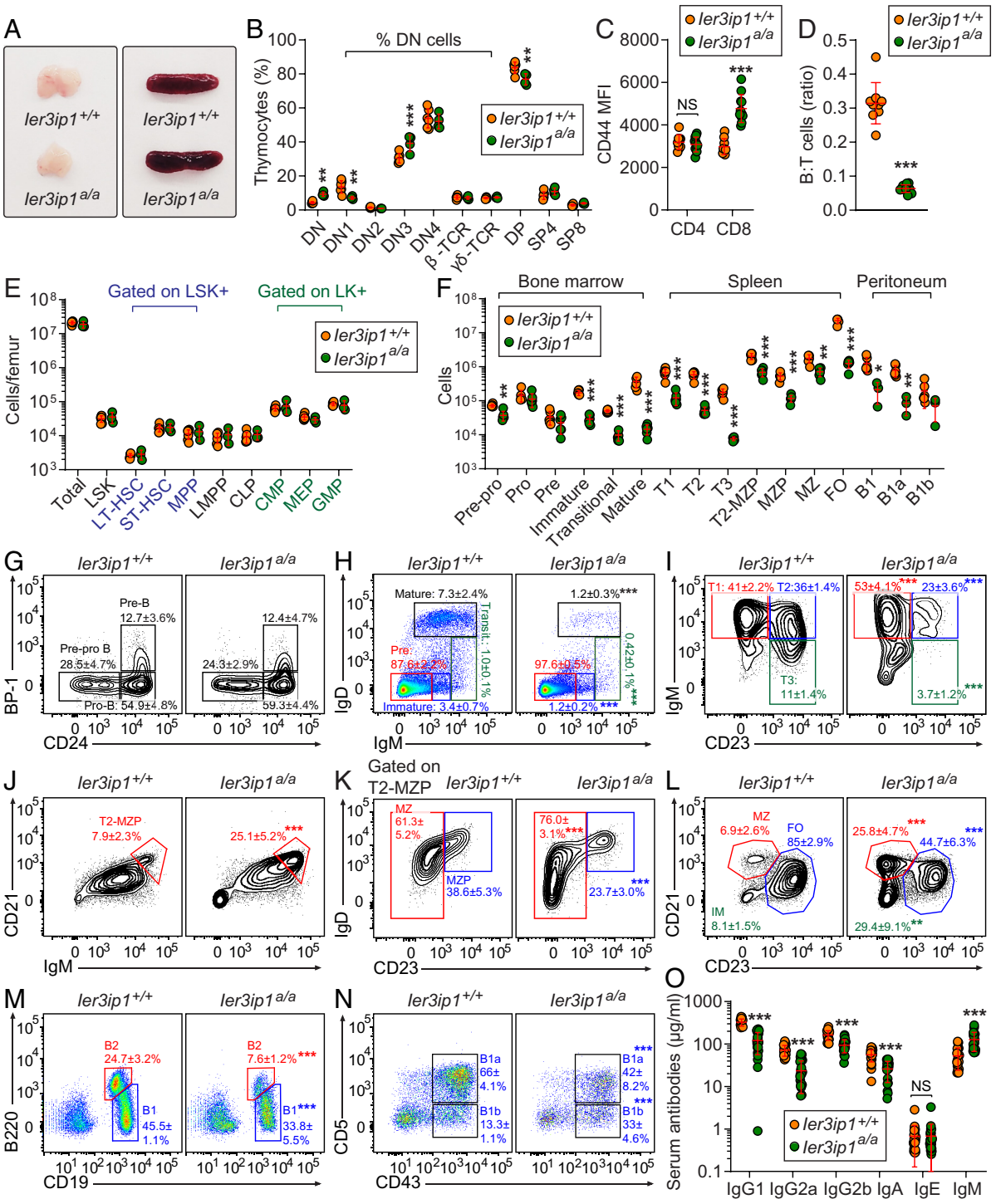

Fig. 2. Severe B cell deficiency caused by an *Ier3ip1* mutation in mice. (*A*) Representative photographs of thymi and spleens isolated from 8-wk-old *Ier3ip1*$^{a/a}$ and wild-type littermates. (*B*) Thymocyte subpopulations in 8-wk-old *Ier3ip1*$^{a/a}$ and wild-type littermates. (n = 4 to 6 mice/genotype). (*C* and *D*) CD44 mean fluorescence intensity (MFI) on CD4$^+$ and CD8$^+$ T cells (*C*) as well as the ratio of B cells to T cells (*D*) in the peripheral blood from 8-wk-old *Ier3ip1*$^{a/a}$ mice and wild-type littermates (n = 9 to 11 mice/genotype). (*E*) Quantitative analysis of the HSC and progenitor populations in the BM of 8- to 10-wk-old *Ier3ip1*$^{a/a}$ and wild-type littermates (n = 3 to 7 mice/genotype). Each cell subset was gated as described previously (15). LT-HSC: long-term hematopoietic stem cells, ST-HSC: short-term hematopoietic stem cells, MPP: multipotent progenitors, LMPP: lymphoid-primed multipotent progenitors, MEP: megakaryocyte–erythroid progenitors, CMP: common myeloid progenitors, and GMP: granulocyte-macrophage progenitors. (*F*) Numbers of B cell subpopulations in the BM, spleen, and peritoneal cavity of 8- to 10-wk-old *Ier3ip1*$^{a/a}$ and wild-type littermates (n = 6 mice/genotype). (*G*–*N*) Representative flow cytometry plots showing B cell development in the BM (*G* and *H*), spleen (*I*–*L*), and peritoneal cavity (*M* and *N*) from 8- to 10-wk-old *Ier3ip1*$^{a/a}$ and wild-type littermates (n = 6 mice/genotype). Each B cell subset was gated as follows: pre-pro-B: B220^{low}Ly51$^-$CD24^{low}, pro-B: B220^{low}Ly51$^-$CD24$^+$, pre-B: B220^{low}Ly51$^+$CD24$^+$, immature B: B220$^+$IgM$^+$IgD$^-$, transitional B: B220$^+$IgM^{high}IgD^{low}, mature recirculating B: B220$^+$IgD$^+$IgM$^+$, T1: B220$^+$CD93$^+$IgM^{high}CD23$^-$, T2: B220$^+$CD93$^+$IgM^{high}CD23$^+$, T3: B220$^+$CD93$^+$IgM^{low}CD23$^+$, follicular B (FOB): B220$^+$CD93$^-$IgM$^+$CD21$^+$CD23^{high}, marginal zone precursor (MZP): B220$^+$CD93$^-$IgM$^+$CD21$^+$CD2a3^{high}, marginal zone B (MZ): B220$^+$CD93$^-$IgM$^+$CD21$^+$CD23^{low}, B2: B220$^+$CD19$^+$, B1: B220^{low}CD19$^+$, B1a: B220^{low}CD19$^+$CD43$^+$CD5$^+$, and B1b: B220^{low}CD19$^+$ CD43$^+$CD5$^-$. Numbers adjacent or inside outlined regions represent percent cells in each. (*O*) Total serum IgG1, IgG2a, IgG2b, IgA, IgE, and IgM were detected in *Ier3ip1*$^{a/a}$and wild-type littermates by ELISA (n = 23 mice/genotype). Data are representative of two (*B*, *E*, *F*, and *G*–*O*) or three independent experiments (*A*, *C*, and *D*). Data points represent individual mice (*B*–*F* and *O*). Error bars indicate SD. *P* values were determined by Student's *t* test (*B*–*O*). *$P < 0.5$; **$P < 0.01$; ***$P < 0.001$; NS, not significant.

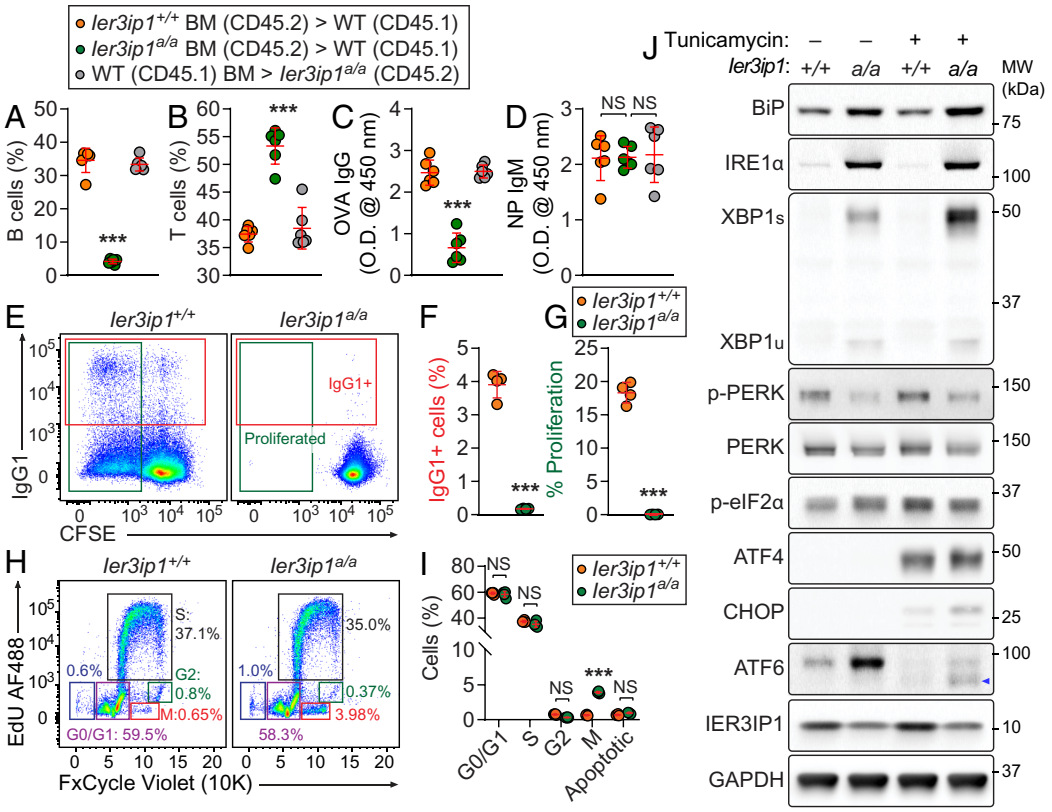

Fig. 3. A cell-intrinsic effect of an *Ier3ip1* mutation on B cell function and UPR. (*A* and *B*) Repopulation of donor-derived B cells (*A*) and T cells (*B*) in the peripheral blood of recipients 12 wk after reconstitution with BM isolated from mice with the indicated genotypes (n = 6 mice/group). (*C* and *D*) T cell–dependent (*C*) and T cell–independent antibody responses (*D*) after immunization with aluminum hydroxide-precipitated OVA and NP-Ficoll, respectively, in the BM chimeras at 10 wk after reconstitution (n = 6 mice/group). Data are represented as absorbance at 450 nm. (*E*–*I*) Flow cytometry analysis of immunoglobulin class switch recombination (*E* and *F*), proliferative response (*E* and *G*), and cell cycle (*H* and *I*) of splenic naive B cells. Splenic naive B cells isolated from *Ier3ip1*$^{a/a}$ and wild-type littermates were stimulated with LPS and IL-4 for 72 h at 37 °C (n = 4 mice/genotype). Numbers adjacent to outlined areas indicate percent cells in each. (*J*) Immunoblot analysis of BiP, IRE1α, XBP1s (spliced), XBP1u (unspliced), p-PERK, PERK, p-eIF2α, ATF4, CHOP, ATF6, IER3IP1, and GAPDH in total cell lysates of splenic pan B cells from *Ier3ip1*$^{a/a}$ and wild-type littermates before and after stimulation with tunicamycin for 4 h at 37 °C. Data are representative of two independent experiments. Data points represent individual mice (*A*–*D*, *F*, *G*, and *I*). Error bars indicate SD. *P* values were determined by one-way ANOVA with Dunnett's multiple comparisons (*A*–*D*) or Student's *t* test (*F*, *G*, and *I*). ***$P < 0.001$; NS, not significant.

Analysis of the IER3IP1 Interactome in B Cells. IER3IP1 was shown to be important for the maintenance of ER homeostasis in the brain and pancreas, dysregulation of which causes MEDS in humans. However, the mechanisms through which IER3IP1 supports ER homeostasis remain unknown. The ready accessibility of pure B cell populations and B cell lines prompted us to investigate the molecular function of IER3IP1 in B cells by identifying its interacting proteins. We generated mouse B cell lines (A20) stably expressing FLAG-tagged IER3IP1 (IER3IP1-FLAG) or empty-FLAG (*SI Appendix*, Fig. S2) using bicistronic internal ribosome entry site-mediated green fluorescent protein reporter expression system (IRES-GFP) containing retroviral vectors (25), and subjected FLAG immunoprecipitates to mass spectrometry analysis. A total of 1,028 candidate proteins were identified from three independent MS analyses; 657 proteins were more abundant in the IER3IP1 immunoprecipitates relative to empty vector control (Fig. 4*A* and Dataset S1). Among these, five were considered candidate IER3IP1 interactors based on their binding affinity to IER3IP1. Four of them were found exclusively in the IER3IP1 co-IP product: myotubularin-related protein 14 (MTMR14), B cell differentiation antigen CD72 (CD72), casein kinase II subunit beta (CSNK2b), and protein kish-A (also known as TMEM167A). Although it was not identified exclusively in the IER3IP1 co-IP, a protein named ORC ubiquitin ligase 1 (also known as RNF219) was also considered a candidate interactor based on the binding affinity to IER3IP1. We also identified Mcl-1 ubiquitin ligase E3 (Mule; also known as HUWE1) as a candidate IER3IP1 interactor, although its binding affinity to IER3IP1 was weak. We attempted to validate the functional relevance of each of these interactions in B cells.

An E3 ubiquitin ligase, HUWE1 functions in maintaining homeostasis of pancreatic β-cells (26) and B cells (27, 28) in mice. HUWE1 is known to promote DNA damage-induced apoptosis by degrading the antiapoptotic BCL2 protein family member MCL1 via the ubiquitin-proteasome pathway (29). In contrast, HUWE1 regulates B cell maturation and function by promoting degradation of p53 which enhances Myc transcription (30). To determine the functional relationship between HUWE1 and IER3IP1, we tested levels of the known HUWE1 substrate MCL1 and other downstream proteins in splenic *Ier3ip1* mutant B cells. Immunoblot analysis showed that reduced IER3IP1 expression had no effect on HUWE1, MCL1, c-Myc, or BCL2 levels in unstimulated or stimulated *Ier3ip1* mutant B cells relative to those in wild-type cells (Fig. 4*B*). This result indicates that reduced IER3IP1 does not alter HUWE1-dependent signaling in *Ier3ip1* mutant B cells.

Another candidate IER3IP1 interactor, CD72, is an inhibitory coreceptor of the B cell receptor (BCR). As in *Ier3ip1*$^{a/a}$ mice, CD72 deficiency in mice has been reported to result in reductions in mature B cells and increases in pre-B cells in the BM, and reduced B-2 cell populations in the peritoneal cavity (31). However, we found increased CD72 expression on *Ier3ip1* mutant B cells compared to wild-type B cells (Fig. 4*C*), suggesting that

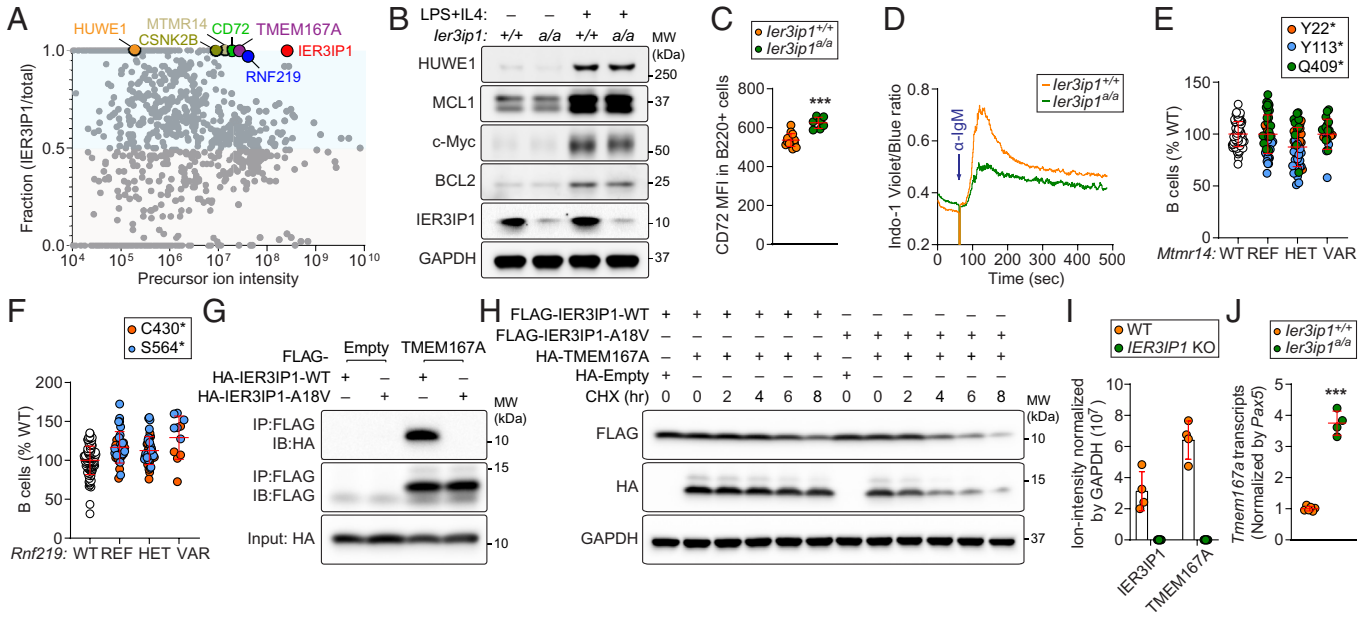

Fig. 4. The IER3IP1 interactome. (*A*) IER3IP1 interactors identified by coimmunoprecipitation combined with liquid Chromatography with tandem mass spectrometry (LC–MS/MS) using mouse B cell lines (A20) stably expressing FLAG-tagged mouse IER3IP1 or empty-FLAG. Relative protein abundance calculated using precursor ion intensities (abundance in IER3IP1 IP ÷ sum of abundances in IER3IP1 and control IP) is plotted on the *y* axis. y = 0.5 indicates equivalent abundance in the IER3IP1 IP and control IP. y > 0.5 indicates enrichment in the IER3IP1 IP, with y = 1 indicating that the protein was exclusively detected in the IER3IP1 IP. *X* axis values represent the precursor ion intensity detected by MS. Data shown are combined from three independent MS analyses (n = 5 IP/cell line). (*B*) Immunoblot analysis of HUWE1, MCL1, c-Myc, BCL2, IER3IP1, and GAPDH in total cell lysates of splenic pan B cells from *Ier3ip1*$^{a/a}$ and wild-type littermates following LPS and IL-4 stimulation for 48 h or left untreated. (*C*) Flow cytometry analysis of CD72 expression on peripheral blood B cells from 8-wk-old *Ier3ip1*$^{a/a}$ and wild-type littermates (n = 7 to 14 mice/genotype). (*D*) Splenic pan B cells from *Ier3ip1*$^{a/a}$ and wild-type littermates were labeled with Indo-1/AM ester. Fluorescence was measured for 60 s to establish a baseline, and then, cells were stimulated with anti-IgM (blue arrowhead). Cytosolic Ca^{2+} flux was monitored with flow cytometry by measuring the ratio of Indo-1 violet and blue fluorescence emission. Kinetic traces are displayed and were normalized to baseline (*n* = 4 mice/genotype). (*E* and *F*) The frequency of peripheral blood B cells from third-generation (G3) descendants of three (*E*) or two (*F*) independent ENU-mutagenized male mice (G1), with REF (+/+), HET (+/mutant), or VAR (mutant/mutant) genotypes for nonsense mutations in *Mtmr14* (*E*, n = 3 to 23 mice/genotype) or *Rnf219* (*F*, n = 5 to 21 mice/genotype), respectively. (*G*) HEK293T cells were transfected with either FLAG-tagged TMEM167A or empty-FLAG, and HA-tagged wild-type IER3IP1 (WT) or mutant IER3IP1 (A18V). Cell lysates were immunoprecipitated using anti-FLAG M2 agarose beads and immunoprecipitates were subsequently analyzed with antibodies against FLAG or HA. (*H*) HEK293T cells were transfected with HA-tagged TMEM167A or empty-HA, and either FLAG-tagged WT or mutant IER3IP1. Fourteen hours after transfection, cells were treated with cycloheximide (CHX) and harvested at indicated times posttreatment. Cell lysates were immunoblotted with indicated antibodies. (*I*) TMEM167A expression in *IER3IP1* knockout human cerebrum organoids. Raw MS data were obtained from the ProteomeXchange dataset with accession number PDX019350 (7). (*J*) Quantitative real-time PCR analysis of *Tmem167* transcript levels in splenic B cells isolated from *Ier3ip1*$^{a/a}$ and wild-type littermates (n = 4 to 6 mice/genotype). Data are representative of one (*E* and *F*), two (*B*–*D*, *G*, *H*, and *J*), or three (*A*) independent experiments. Data points represent individual mice (*C*, *E*, *F*, and *J*) or organoids with indicated genotype (*I*). Error bars indicate SD. *P* values were determined by Student's *t* test (*C* and *J*) or one-way ANOVA with Dunnett's multiple comparisons (*E* and *F*). ***$P < 0.001$.

CD72 did not mediate the effects of the IER3IP1 mutation on B cell development. On the other hand, CD72 deficiency enhanced Ca^{2+} flux upon BCR cross-linking and resulted in B cell hyperproliferation in response to polyclonal stimulation by LPS (31). Consistent with increased CD72 expression, the *alarmist* mutation impaired Ca^{2+} flux following BCR cross-linking (Fig. 4*D*) and significantly inhibited B cell proliferation upon polyclonal stimulation (Fig. 3 *D* and *F*). We note that others have reported no change in these responses in *Cd72*$^{-/-}$ B cells with respect to WT B cells (32). Thus, we concluded that elevated CD72 may mediate some effects of IER3IP1 deficiency in B cells, but it does not account for all aspects of the B cell phenotype in *Ier3ip1*$^{a/a}$ mice.

We also concluded that three other putative interactors are irrelevant to the role of IER3IP1 in B cell development for the following reasons: i) CSNK2B: Mutations in *CSNK2B*, which encodes the β subunits of CK2, cause epilepsy in humans (33). Unlike *IER3IP1* variants, *CSNK2B* mutations do not result in microcephaly (34). Conditional *Csnk2b* deletion causes cell cycle arrest at the S phase. However, *Ier3ip1* mutation results in cell cycle arrest at the M phase (Fig. 3*G*). ii) MTMR14: As a member of the MTM-related protein family, MTMR14 controls the excitation–contraction-relaxation process of muscle by regulating store operated Ca^{2+} entry [SOCE; (35)]. In our forward genetic screen, we screened three pedigrees harboring nonidentical MTMR14 nonsense alleles (tyrosine to stop codon at position 22: Y22*, tyrosine to stop codon at position 113: Y113*, glutamine to stop codon at position 409: Q409*; full-length mouse MTMR14: 648 aa) and found normal B cell development in these mutant mice (superpedigree *P*-value: additive model: 9.67E-02, recessive model: 8.37E-01, dominant model: 1.99E-02; Fig. 4*E*). iii) RNF219: Localized in the nucleus, the RING-type E3 ligase RNF219 controls translational repression by inhibiting CCR4-NOT, the major mRNA deadenylase responsible for 3′ poly(A) tail shortening and therefore essential in maintaining normal rates of mRNA turnover (36, 37). We also screened two pedigrees carrying nonidentical RNF219 nonsense alleles (cysteine to stop codon at position 430: C430* and serine to stop codon at position 564: S564*; full-length mouse RNF219: 722 aa) and found normal B cell development in these mutant mice (superpedigree *P*-value: additive: 2.87E-01, recessive: 3.06E-02, dominant: 9.95E-01; Fig. 4*F*).

The last IER3IP1 interactor tested in the present study is TMEM167A (also known as protein kish-A). Localized in the Golgi apparatus membrane, the protein is known to function in the early part of the protein secretory pathway. Furthermore, knockdown of TMEM167A together with paralogue TMEM167B resulted in reduction of protein secretion in a cell line expressing a regulated secretory reporter (38, 39). This finding caught our attention because IER3IP1 is necessary for extracellular matrix

protein secretion in human cerebral organoid tissue, and IER3IP1 deficiency impairs tissue integrity and brain development (7). Since the two proteins have functional similarity, we tested the effect of the IER3IP1^{A18V} mutation on the binding of TMEM167A. HEK293T cells were transfected with either HA-tagged wild-type or mutant IER3IP1 (A18V), FLAG-tagged TMEM167A, or empty vector alone. Total cell lysates were mixed in vitro and subjected to coimmunoprecipitation using anti-FLAG M2 agarose beads. HA-tagged wild-type IER3IP1 was immunoprecipitated with FLAG-tagged TMEM167A proteins. However, no interaction was found between IER3IP1^{A18V} and TMEM167A (Fig. 4*G*). To test the effect of IER3IP1^{A18V} on TMEM167A stability, HEK293T cells were transfected with FLAG-tagged wild-type or mutant IER3IP1 and HA-tagged TMEM167A or empty vector and subjected to CHX chase analysis. TMEM167A had slower decay kinetics when coexpressed with wild-type IER3IP1 than when it was expressed with the mutant IER3IP1 (Fig. 4*H*).

We also re-searched published proteomic data obtained from *IER3IP1* KO or WT human cerebrum organoids to determine the effect of IER3IP1 deficiency on TMEM167A (7). Strikingly, near complete loss of TMEM167A in *IER3IP1* KO tissues was observed (Fig. 4*I* and Dataset S2). Considering the effect of the *alarmist* mutation (A18V) on IER3IP1 expression (Fig. 1*G*) and TMEM167A binding (Fig. 4*G*), as well as the effect of IER3IP1 deficiency on TMEM167A expression, we conclude that IER3IP1 is critical to support TMEM167A stability. We found elevated *Tmem167a* transcript levels in *Ier3ip1* mutant B cells compared to wild-type cells (Fig. 4*J*). We interpret this to be a compensatory mechanism to maintain steady state TMEM167A expression in the mutant cells.

Discussion

IER3IP1 is a highly conserved protein that is found in humans and mice (80 of 82 identical amino acids or 97.56% sequence identity, Fig. 1*C*) and is highly expressed in multiple tissues (8). To date, ten cases of MEDS caused by mutations in human *IER3IP1* have been reported. These include a homozygous valine (V) to glycine (G) substitution at position 21 [V21G; 2 cases; (9, 40)], a homozygous leucine (L) to proline (P) substitution at position 78 [L78P; 6 cases; (9–11)], compound heterozygous V21G and a frameshift deletion after serine 25 [V21G/S25*; (13)], and a very recently reported homozygous variant identical to the *alarmist* mutation [A18V; (12); Fig. 1*C*]. These natural variants and the ENU-induced mutations we identified affect residues in one of the two transmembrane domains of mouse or human IER3IP1 (Fig. 1*C*). Although recent studies suggested roles for IER3IP1 in maintaining normal ER function, lack of a viable mouse model to study the pathophysiology of MEDS has hampered understanding of the molecular mechanism(s) by which *IER3IP1* mutations lead to disease. Furthermore, the significance of IER3IP1 in immunity had escaped notice.

Through a forward genetic screen of mice with mutations induced by ENU, we have identified two viable *Ier3ip1* mutations and demonstrated that IER3IP1 is essential for B cell development in mice. Similar to the effect of IER3IP1 deficiency in pancreatic β cells, we found strong activation of the IRE1α-XBP1 dependent UPR in *Ier3ip1*$^{a/a}$ splenic B cells even at steady state indicating that the A18V mutation also led to ER dysfunction in immune cells. The UPR signaling pathway helps cells cope with ER stress by activating a genetic program that leads to the rescue or degradation of unfolded proteins within the ER. In B cells, the IRE1α-XBP1 branch of the UPR signaling pathway is active during B cell development and terminal differentiation (41). In this regard, IRE1α deficiency resulted in blockade of B cell development beyond the pre-B cell stage as well as defective BCR expression that affected differentiation (42). On the other hand, IRE1α serves as a scaffold to form a complex with TRAF2 and ASK1 in response to UPR activation, which subsequently activates JNK-mediated apoptosis (43). It is interesting that the UPR pathway is also active during T cell development and in peripheral CD8+ T cells (41). However, physiological effects of IRE1α during T cell development were not as obvious as in B cells, in that T cell–specific IRE1α deletion did not affect T cell development or activation (44). Our results are consistent with these findings: the A18V mutation in IER3IP1 significantly impaired B cell development (Fig. 2*F*) and function (Figs. 2*O* and 3*D*); however, T cell pools in *alarmist* mice remained unaffected except in the cases of thymic DP cells and peripheral CD8+ T cells (Fig. 2 *B* and *C*, respectively). A question arising from this study is why B cells are particularly affected by IER3IP1 mutations. It is unclear why activation of the UPR is detrimental to developing B cells but relatively well tolerated in developing T cells. As mentioned above, T cells do not appear to require IRE1α for development or function (44), whereas B cells do; thus, we speculate that B cells may be more sensitive than T cells to IRE1α activity, which may trigger developing B cell death. Answering these questions would improve our understanding of ER homeostasis in lymphocyte development and function.

The yeast homolog of IER3IP1, YOS1, localizes in both the ER and Golgi apparatus membranes and is packaged into the membrane of ER-derived COPII vesicles that transfer secretory proteins from ER to Golgi (45). In agreement, IER3IP1 deficiency impairs protein secretion (7), but the mechanism through which IER3IP1 regulates the secretory pathway remains unknown. By determining the IER3IP1 interactome, we found that IER3IP1 binds to the Golgi apparatus membrane protein TMEM167A, which is also known to function in the protein secretory pathway (39). We found that the A18V mutation in *Ier3ip1* not only destabilized IER3IP1 resulting in reduced cellular protein abundance, but also completely abolished binding to TMEM167A. Remarkably, complete IER3IP1 deficiency significantly decreased TMEM167A levels in human cerebrum organoid tissues, suggesting that IER3IP1-TMEM167A interaction is critical to support TMEM167A stability. Considering that yeast YOS1 is a component of the COPII vesicle, it may be that IER3IP1 and TMEM167A are brought together when IER3IP1-containing COPII vesicles are transported to the Golgi membrane containing TMEM167A. Furthermore, the IER3IP1-TMEM167A interaction may facilitate docking or fusion of COPII vesicles with the Golgi apparatus. Our findings (Figs. 2*O* and 3*C*) suggest that terminally differentiated plasma cells may depend on these events to properly secrete antibodies during an immune response. ER stress and cell death may be consequences of disrupted ER-to-Golgi COPII vesicle trafficking resulting from failure of IER3IP1-TMEM167A interaction.

Given the widespread expression of IER3IP1 and TMEM167A, we consider it likely that the complex may serve a similar function in multiple tissues. In view of the strong phenotypic effect and importance of IER3IP1 in diverse cellular processes, the viable *Ier3ip1* missense allele described here will be useful to researchers in many fields.

Materials and Methods

Mice. As written in our previous paper (46), "Eight- to ten-week-old pure C57BL/6J male mice purchased from The Jackson Laboratory were mutagenized with ENU as described previously (47). Mutagenized G0 males were bred to C57BL/6J females, and the resulting G1 males were crossed to C57BL/6J females to produce G2 mice. G2 females were backcrossed to their G1 sires to yield G3 mice, which were screened for phenotypes. Whole-exome sequencing

and meiotic mapping were performed as described (18)." C57BL/6.SJL (CD45.1) mice were purchased from The Jackson Laboratory. All animal work described in this manuscript has been approved by the UT Southwestern Institutional Animal Care and Use Committee.

Flow Cytometry. As written in our previous paper (48), "Peripheral blood was collected from mice >6 wk old by cheek bleeding. Red blood cells (RBCs) were lysed with hypotonic buffer (eBioscience). Samples were washed with FACS staining buffer [Phosphate-buffered saline with 1% (w/v) bovine serum albumin] one time at 500 × g for 5 min. The RBC-depleted samples were stained for 1 h at 4 °C, in 100 μL of 1:200 cocktail of fluorescence-conjugated antibodies to 15 cell surface markers encompassing the major immune lineages: B220 (BD, clone RA3-6B2), CD19 (BD, clone 1D3), IgM (BD, clone R6-60.2), IgD (BioLegend, clone 11-26c.2a), CD3ε (BD, clone 145-2C11), CD4 (BD, clone RM4-5), CD8α (BioLegend, clone 53-6.7), CD11b (BioLegend, clone M1/70), CD11c (BD, clone HL3), F4/80 (Tonbo, clone BM8.1), CD44 (BD, clone 1M7), CD62L (Tonbo, clone MEL-14), CD5 (BD, clone 53-7.3), CD43 (BD, clone S7), NK 1.1 (BioLegend, clone OK136) and 1:200 Fc block (Tonbo, clone 2.4G2)." Mean fluorescence intensity of CD72 in peripheral blood B cells of *Ier3ip1*$^{a/a}$ or wild-type littermates were analyzed using anti-mouse CD72 antibodies (BD, clone K10.6).

BM cells, thymocytes, splenocytes, or peritoneal cells were isolated and prepared for flow cytometry as written in our previous papers (15, 16), "Cells were stained at 1:200 antibody dilution in the presence of anti-mouse CD16/32 antibody (Tonbo, clone 2.4G2) and different antibody cocktails: B cells in BM [IgM (BD, clone R6-60.2), IgD (BioLegend, clone 11-26c.2a), B220 (BD, clone RA3-6B2), CD43 (BD, clone S7), CD5 (BD, clone 53-7.3), CD24 (BioLegend, clone M1/69), Ly-51 (BD, clone BP-1), CD19 (BD, clone 1D3)]; splenic B cells [CD4 (BD, clone RM4-5), IgM (BD, clone R6-60.2), IgD (BioLegend, clone 11-26c.2a), B220 (BD, clone RA3-6B2), CD23 (BD, clone B3B4), CD21/CD35 (BioLegend, clone 7E9), CD93 (BD, clone AA4.1)]; thymocytes [TCRβ (BD, clone H57-597), TCR γ/δ (BioLegend, clone GL3), CD25 (BioLegend, clone 3C7), CD44 (BD, clone 1M7), CD4 (BD, clone RM4-5), CD8α (BioLegend, clone 53-6.7), CD69 (eBioscience, clone H1.2F3)]. The BM HSPCs were stained with Alexa Fluor 700 anti-mouse lineage cocktail (BioLegend, clones 17A2/RB6-8C5/RA3-6B2/Ter-119/M1/70), CD34 (eBioscience, clone RAM34), CD135 (BioLegend, clone A2F10), CD16/CD32 (eBioscience, clone 93), CD127 (BD, clone SB/199), Ly-6A/E (Sca-1) (BioLegend, clone D7), CD117 (c-kit) (BioLegend, clone 2B8). Data were collected on a BD LSRFortessa$^{TM\ cell\ analyzer}$ and the immune cell populations in each mouse were analyzed with FlowJo software."

BM Transplantation. BM chimeras were prepared as described previously (14, 16, 46). Recipient mice were lethally irradiated by giving 7 Gy (1 Gy = 100 rads) via gamma radiation (X-RAD 320 Precision X-Ray; Accela) twice at a 5-h interval. Freshly isolated BM cells were prepared from femurs of C57BL/6.SJL (CD45.1), *Ier3ip1*$^{a/a}$ (CD45.2) homozygotes, or their wild-type littermates (*Ier3ip1*$^{+/+}$, CD45.2). The following transfers were performed: 1) BM cells from *Ier3ip1*$^{a/a}$ (CD45.2) homozygotes, or their wild-type littermates were transferred into irradiated CD45.1 recipients through retro-orbital injection. 2) BM cells from C57BL/6.SJL (CD45.1) mice were injected into irradiated *Ier3ip1*$^{a/a}$ (CD45.2) homozygotes through retro-orbital injection. Mice were maintained on antibiotic water for 4 wk posttransplantation. To determine hematopoietic recovery in recipients, peripheral blood B cells were collected 12 wk posttransplantation. Cells were then stained with fluorescence-conjugated antibodies against the CD45 congenic markers [CD45.1 (BioLegend, clone A10) and CD45.2 (BioLegend, clone 104)] and analyzed by flow cytometry as described above.

Blood/Serum Chemistries and Analysis of Serum Immunoglobulins. Blood glucose levels were measured with the AlphaTRAK glucometer and test strips (Zoetis). Serum insulin levels were measured by ELISA according to the manufacturer's instructions (Crystal Chem). Serum IgG1, IgG2a, IgG2b, IgA, IgE, and IgM concentrations in *Ier3ip1*$^{a/a}$ and *Ier3ip1*$^{+/+}$ littermates were also analyzed by ELISA according to the manufacturer's instructions (Bethyl laboratories, Thermo Fisher Scientific).

Histology. Hematoxylin and eosin staining and insulin immunohistochemistry of pancreases isolated from *Ier3ip1*$^{a/a}$ or wild-type littermates were performed using standard procedures by UT Southwestern Histology Core.

Cell Culture, Coimmunoprecipitation, and Immunoblotting. Basic biochemistry experiments were performed as written in our previous paper (16), "HEK293T cells were grown at 37 °C in Dulbecco's Modified Eagle Medium (Life Technologies)/10% (v/v) fetal bovine serum (Gibco)/1% antibiotics (Life Technologies) in 5% CO_2. Transfection of plasmids was carried out using Lipofectamine 2000 (Life Technologies) according to the manufacturer's instructions. 36 to 48 h after transfection, cells were harvested in NP- 40 lysis buffer (20 mM Tris–Cl, pH 7.5, 150 mM NaCl, 1 mM Ethylenediaminetetraacetic acid, 1 mM Ethyleneglycol- bis(β-aminoethyl)-N,N,N′,N′-tetraacetic Acid, 1% (v/v) NP-40, 2.5 mM $Na_4P_2O_7$, 1 mM $C_3H_9O_6P$, 1 mM Na_3VO_4, and protease inhibitors) for 45 min at 4 °C.

For standard immunoblot analysis, cells were lysed in buffer [1% sodium dodecyl sulfate (Thermo Fisher), 1:10,000 Benzonase (Sigma), 1:100 Protease Inhibitor Cocktail (Cell Signaling Technology: CST), in buffer A (50 mM 4-(2-hydroxyethyl)-1-piperazineethanesulfonic acid, 2 mM $MgCl_2$, 10 mM KCl)]. Protein concentration was measured using the BCA assay (Pierce). Equal amounts (~20 μg) of protein extracts were separated by electrophoresis on 4 to 12% Bis-Tris mini gels (Life Technologies) and transferred to nitrocellulose membranes (Bio-Rad). After blocking in Tris-buffered saline containing 0.05% Tween-20 (TBS-T) with 5% (w/v) non-fat dry milk at room temperature for 1 h, the membrane was incubated overnight with primary antibody [anti-FLAG (Sigma Aldrich, clone M2), anti-IER3IP1 (Invitrogen, PIPA569453), anti-BiP (CST, clone C50B12), anti- IRE1α (CST, clone 14C10), anti-XBP1 (Abcam, ab220783), anti-PERK (CST, clone C33E10), anti-phospho-PERK (CST, clone 16F8), anti-phospho-eIF2α (CST, clone D9G8), anti-ATF4 (CST, clone D4B8), anti-ATF6 (CST, clone D4Z8V), anti-CHOP (CST, clone D46F1), anti-HUWE1 (Abcam, ab271032), anti-MCL1 (CST, clone D2W9E), anti-Myc (CST, clone D84C12), anti-BCL2 (CST, clone D17C4), anti-PLCγ2 (CST, #3872), and anti-GAPDH (CST, clone D16H11)] at 4 °C in 5% (w/v) BSA in TBS-T with gentle rocking. The membrane was then incubated with secondary antibody [goat anti-mouse IgG-HRP (Southern Biotech), or goat anti-rabbit IgG-HRP (Thermo Fisher Scientific)] for 1 h at room temperature. The chemiluminescence signal was developed by using SuperSignal West Dura Extended Duration Substrate kit (Thermo Scientific) and detected by a G:Box Chemi XX6 system (Syngene)."

Coimmunoprecipitation assays were performed using cell extracts from HEK293T cells overexpressing FLAG-tagged wild-type or mutant (A18V) IER3IP1, or HA-tagged TMEM167A proteins in separate cultures. Extracts of cells expressing the proteins of interest were mixed and incubated overnight at 4 °C. Immunoprecipitation was performed by anti-Flag M2 affinity gel (Sigma Aldrich) as previously described (15), and standard immunoblot was performed as described above.

CHX chase assay was performed as described in our previous paper (49).

ER Stress Measurement. Splenic pan B cells were isolated using the EasySep Mouse B Cells Isolation Kit (StemCell Technologies). Cells were treated with tunicamycin (3.3 μg/mL, CST) for 4 h at 37 °C. Cells were harvested and lysed in 1% SDS lysis buffer. ER stress induction was analyzed by assessing protein expression levels with indicated antibodies using standard immunoblot assay as described above.

In Vitro Class Switching and Cell Cycle Analysis. Splenic naive B lymphocytes were isolated from *Ier3ip1*$^{a/a}$ or wild-type littermates using anti-CD43 MicroBeads (Miltenyi Biotec). Cells were stained with 5 μM CellTrace CFSE (Life Technologies) and stimulated to undergo class switching to IgG1 with 25 μg/mL LPS (Sigma Aldrich) and 10 ng/mL of mouse recombinant IL-4 (BioLegend) for 72 h at 37 °C. For cell cycle analysis, splenic naive B cells were stimulated with LPS and IL-4 as described above for 72 h at 37 °C. Cells were then labeled with the Click-iT EdU Flow Cytometry Assay Kit (Invitrogen) according to the manufacturer's instructions. DNA content stain was performed using FxCycle Violet dye (Invitrogen). In vitro class switching and cell cycle were analyzed by flow cytometry.

Generation of a Mouse B Cell Line Stably Expressing FLAG-Tagged IER3IP1. PT67 cells (ATCC) were transfected with FLAG-tagged IER3IP1 (NM_025409.1)-pMSCV-IRES-GFP or empty vector [pMSCV-IRES-GFP, (25)] using Lipofectamine 2000 (Life Technologies). Green fluorescent protein (GFP)-expressing PT67 cells were sorted using an Aria II cell sorter (BD). Retroviruses recovered from the media of PT67 cells were concentrated by Retro-X concentrator according to the manufacturer's instructions (Takara) and used to infect mouse B cell line A20 (ATCC) with polybrene (4 μg/mL). Forty-eight hours later, GFP-expressing A20 cells were sorted by flow cytometry. The A20 cells stably expressing FLAG-tagged IER3IP1 were used for immunoprecipitation assay as described above. Immunoprecipitates were digested for IER3IP1 interactome analysis using MS as described below.

Protein Digestion and MS. As written in ref. 50, "Protein was solubilized in 8 M urea 100 mM Tris pH 8.5 and reduced with 5 mM Tris (2-carboxyethyl) phosphine hydrochloride (Sigma Aldrich) and alkylated with 55 mM 2-Chloroacetamide (Sigma Aldrich). Proteins were digested for 18 h at 37 °C in 2 M urea 100 mM Tris pH 8.5, with 0.5 μg trypsin (Promega). Single phase analysis was performed using a Q Exactive HF Orbitrap Mass Spectrometer (Thermo Scientific). Protein and peptide identification were done with MSFragger [version 14.0; https://fragpipe.nesvilab.org/; (51)] using a mouse protein database downloaded from UniProt (uniprot.org; 11/15/2022, 21,986 entries), common contaminants and reversed sequences added. The search space included all fully tryptic peptide candidates with a fixed modification of 57.021464 on C, variable modification of 15.9979 on M and 42.0106 on the N-terminus. MS1 quantification was done with total intensity and no match between runs. Protein intensity values were combined for replicates."

Reanalysis of Published Proteomic Data from *IER3IP1* Knockout Human Cerebrum Organoids. Raw files were downloaded for Project PXD019350 from ProteomeXchange. As written in ref. 50, "Protein and peptide identification were done with MSFragger within the FragPipe Pipeline [https://fragpipe.nesvilab.org/; (51)] using a human protein database downloaded from UniProt (uniprot.org; 1/2/2023, 20,594 entries), common contaminants and reversed sequences added. The search space included all fully tryptic peptide candidates with a fixed modification of 57.021464 on C, variable modification of 15.9979 on M and 42.0106 on the N-terminus. MS1 quantification was done with total intensity and match between runs."

Ca^{2+} Flux Measurement. To monitor changes in Ca^{2+} flux, 10^7 freshly isolated splenic pan B cells in 1 mL of RPMI 1640 containing 2% fetal bovine serum and 10 mM 4-(2-hydroxyethyl)-1-piperazineethanesulfonic acid (HEPES) (R2 medium) were loaded with 1 μM indo-1/AM ester (Molecular Probes) for 30 min at 37 °C. Cells were then washed and diluted at 2 × 10^6/mL in R2 medium. The ratio of indo-1 violet/blue in response to treatment with anti-IgM (Invitrogen) was analyzed by flow cytometry.

Plasmids. Mouse IER3IP1^{WT} (NM_025409.1) and IER3IP1^{A18V} were tagged N-terminally with HA epitope in the pCMV6 vector. Full-length mouse TMEM167A (NM_025335) with FLAG epitope were cloned into pCDNA6 vector. All plasmids were verified by capillary sequencing.

Quantitative RT-PCR. Total RNA from splenic pan B cells from *Ier3ip1*$^{a/a}$ or WT littermates was prepared using the RNeasy Mini Kit according to the manufacturer's instructions (Qiagen) and treated with RQ1 RNase-free DNase I (Promega) at 37 °C for 30 min to remove contaminating genomic DNA. Equal amounts (200 ng) of RNA were used for reverse transcription using an oligo (dT) primer (Promega). Quantitative RT-PCR was performed with the following primer pairs: *Tmem167a* forward: CATGATGGACCAGGGAACTAAA, reverse: CCTCCGGGACAATTCAAGATAA; *Pax5* forward: CGAGTCTGTGACAATGACACTGTGC, reverse: CAGGATGCCACTGATGGAGTATG.

Statistical Analysis. The statistical significance of differences between two or more groups was analyzed with GraphPad Prism using the indicated analyses in each figure. Differences in values were considered statistically significant when $P < 0.05$. P values are denoted by $*P < 0.05$; $**P < 0.01$; $***P < 0.001$; and NS, not significant with $P > 0.05$.

Data, Materials, and Software Availability. Raw MS data have been deposited in the MassIVE repository (https://massive.ucsd.edu/ProteoSAFe/dataset.jsp?accession=MSV000091025) with accession no. MSV000091025 (52).

ACKNOWLEDGMENTS. We thank the UTSW Proteomics Core facility for assistance with proteomics experiments. This work was supported by the NIH (AI125581 to B.B.).

1. R. R. Hardy, K. Hayakawa, B cell development pathways. *Annu. Rev. Immunol.* **19**, 595–621 (2001).
2. A. L. Shaffer *et al.*, XBP1, downstream of Blimp-1, expands the secretory apparatus and other organelles, and increases protein synthesis in plasma cell differentiation. *Immunity* **21**, 81–93 (2004).
3. N. N. Iwakoshi *et al.*, Plasma cell differentiation and the unfolded protein response intersect at the transcription factor XBP-1. *Nat. Immunol.* **4**, 321–329 (2003).
4. A. Li, N. J. Song, B. P. Riesenberg, Z. Li, The emerging roles of endoplasmic reticulum stress in balancing immunity and tolerance in health and diseases: Mechanisms and opportunities. *Front. Immunol.* **10**, 3154 (2019).
5. J. Sun, D. Ren, IER3IP1 deficiency leads to increased beta-cell death and decreased beta-cell proliferation. *Oncotarget* **8**, 56768–56779 (2017).
6. J. Yang *et al.*, IER3IP1 is critical for maintaining glucose homeostasis through regulating the endoplasmic reticulum function and survival of beta cells. *Proc. Natl. Acad. Sci. U.S.A.* **119**, e2204443119 (2022).
7. C. Esk *et al.*, A human tissue screen identifies a regulator of ER secretion as a brain-size determinant. *Science* **370**, 935–941 (2020).
8. W. H. Yiu, J. W. Poon, S. K. Tsui, K. P. Fung, M. M. Waye, Cloning and characterization of a novel endoplasmic reticulum localized G-patch domain protein, IER3IP1. *Gene* **337**, 37–44 (2004).
9. C. J. Poulton *et al.*, Microcephaly with simplified gyration, epilepsy, and infantile diabetes linked to inappropriate apoptosis of neural progenitors. *Am. J. Hum. Genet.* **89**, 265–276 (2011).
10. G. M. Abdel-Salam *et al.*, A homozygous IER3IP1 mutation causes microcephaly with simplified gyral pattern, epilepsy, and permanent neonatal diabetes syndrome (MEDS). *Am. J. Med. Genet. A.* **158A**, 2788–2796 (2012).
11. I. Valenzuela *et al.*, Microcephaly with simplified gyral pattern, epilepsy and permanent neonatal diabetes syndrome (MEDS). A new patient and review of the literature. *Eur. J. Med. Genet.* **60**, 517–520 (2017).
12. E. Sobu, G. D. Kaya Ozcora, E. Yilmaz Gulec, B. Sahinoglu, F. Tahmiscioglu Bucak, A new variant of the IER3IP1 gene: The first case of microcephaly, epilepsy, and diabetes syndrome 1 from Turkey. *J. Clin. Res. Pediatr. Endocrinol.*, 10.4274/jcrpe.galenos.2022.2022-8-12 (2022).
13. S. A. Shalev *et al.*, Microcephaly, epilepsy, and neonatal diabetes due to compound heterozygous mutations in IER3IP1: Insights into the natural history of a rare disorder. *Pediatr. Diabetes* **15**, 252–256 (2014).
14. J. H. Choi *et al.*, LMBR1L regulates lymphopoiesis through Wnt/beta-catenin signaling. *Science* **364**, eaau0812 (2019).
15. J. H. Choi *et al.*, Essential requirement for nicastrin in marginal zone and B-1 B cell development. *Proc. Natl. Acad. Sci. U.S.A.* **117**, 4894–4901 (2020).
16. J. H. Choi *et al.*, Essential cell-extrinsic requirement for PDIA6 in lymphoid and myeloid development. *J. Exp. Med.* **217**, e20190006 (2020).
17. D. Xu *et al.*, Thousands of induced germline mutations affecting immune cells identified by automated meiotic mapping coupled with machine learning. *Proc. Natl. Acad. Sci. U.S.A.* **118**, e2106786118 (2021).
18. T. Wang *et al.*, Real-time resolution of point mutations that cause phenovariance in mice. *Proc. Natl. Acad. Sci. U.S.A.* **112**, E440–E449 (2015).
19. I. A. Adzhubei *et al.*, A method and server for predicting damaging missense mutations. *Nat. Methods* **7**, 248–249 (2010).
20. F. Martin, A. M. Oliver, J. F. Kearney, Marginal zone and B1 B cells unite in the early response against T-independent blood-borne particulate antigens. *Immunity* **14**, 617–629 (2001).
21. K. Kohno, K. Normington, J. Sambrook, M. J. Gething, K. Mori, The promoter region of the yeast KAR2 (BiP) gene contains a regulatory domain that responds to the presence of unfolded proteins in the endoplasmic reticulum. *Mol. Cell Biol.* **13**, 877–890 (1993).
22. J. S. Cox, C. E. Shamu, P. Walter, Transcriptional induction of genes encoding endoplasmic reticulum resident proteins requires a transmembrane protein kinase. *Cell* **73**, 1197–1206 (1993).
23. H. P. Harding, Y. Zhang, D. Ron, Protein translation and folding are coupled by an endoplasmic-reticulum-resident kinase. *Nature* **397**, 271–274 (1999).
24. J. Shen, R. Prywes, ER stress signaling by regulated proteolysis of ATF6. *Methods* **35**, 382–389 (2005).
25. J. Holst *et al.*, Generation of T-cell receptor retrogenic mice. *Nat. Protoc.* **1**, 406–417 (2006).
26. N. Kon, J. Zhong, L. Qiang, D. Accili, W. Gu, Inactivation of arf-bp1 induces p53 activation and diabetic phenotypes in mice. *J. Biol. Chem.* **287**, 5102–5111 (2012).
27. Z. Hao *et al.*, The E3 ubiquitin ligase Mule acts through the ATM-p53 axis to maintain B lymphocyte homeostasis. *J. Exp. Med.* **209**, 173–186 (2012).
28. B. King *et al.*, The ubiquitin ligase Huwe1 regulates the maintenance and lymphoid commitment of hematopoietic stem cells. *Nat. Immunol.* **17**, 1312–1321 (2016).
29. Q. Zhong, W. Gao, F. Du, X. Wang, Mule/ARF-BP1, a BH3-only E3 ubiquitin ligase, catalyzes the polyubiquitination of Mcl-1 and regulates apoptosis. *Cell* **121**, 1085–1095 (2005).
30. C. F. Qi *et al.*, Homeostatic defects in B cells deficient in the E3 ubiquitin ligase ARF-BP1 are restored by enhanced expression of MYC. *Leuk. Res.* **37**, 1680–1689 (2013).
31. C. Pan, N. Baumgarth, J. R. Parnes, CD72-deficient mice reveal nonredundant roles of CD72 in B cell development and activation. *Immunity* **11**, 495–506 (1999).
32. M. Xu *et al.*, Cd72(c) is a modifier gene that regulates Fas(lpr)-induced autoimmune disease. *J. Immunol.* **190**, 5436–5445 (2013).
33. M. Nakashima *et al.*, Identification of de novo CSNK2A1 and CSNK2B variants in cases of global developmental delay with seizures. *J. Hum. Genet.* **64**, 313–322 (2019).
34. J. Li *et al.*, Germline de novo variants in CSNK2B in Chinese patients with epilepsy. *Sci. Rep.* **9**, 17909 (2019).
35. J. Shen *et al.*, Deficiency of MIP/MTMR14 phosphatase induces a muscle disorder by disrupting Ca(2+) homeostasis. *Nat. Cell Biol.* **11**, 769–776 (2009).
36. A. Guenole *et al.*, RNF219 regulates CCR4-NOT function in mRNA translation and deadenylation. *Sci. Rep.* **12**, 9288 (2022).
37. F. Poetz *et al.*, RNF219 attenuates global mRNA decay through inhibition of CCR4-NOT complex-mediated deadenylation. *Nat. Commun.* **12**, 7175 (2021).
38. V. M. Rivera *et al.*, Regulation of protein secretion through controlled aggregation in the endoplasmic reticulum. *Science* **287**, 826–830 (2000).
39. F. Wendler *et al.*, A genome-wide RNA interference screen identifies two novel components of the metazoan secretory pathway. *EMBO J.* **29**, 304–314 (2010).
40. K. Rjiba *et al.*, Further report of MEDS syndrome: Clinical and molecular delineation of a new Tunisian case. *Eur. J. Med. Genet.* **64**, 104285 (2021).
41. R. Brunsing *et al.*, B- and T-cell development both involve activity of the unfolded protein response pathway. *J. Biol. Chem.* **283**, 17954–17961 (2008).

42. K. Zhang *et al.*, The unfolded protein response sensor IRE1alpha is required at 2 distinct steps in B cell lymphopoiesis. *J. Clin. Invest.* **115**, 268–281 (2005).
43. F. Urano *et al.*, Coupling of stress in the ER to activation of JNK protein kinases by transmembrane protein kinase IRE1. *Science* **287**, 664–666 (2000).
44. K. L. Kemp *et al.*, The serine-threonine kinase inositol-requiring enzyme 1alpha (IRE1alpha) promotes IL-4 production in T helper cells. *J. Biol. Chem.* **288**, 33272–33282 (2013).
45. M. Heidtman, C. Z. Chen, R. N. Collins, C. Barlowe, Yos1p is a novel subunit of the Yip1p-Yif1p complex and is required for transport between the endoplasmic reticulum and the Golgi complex. *Mol. Biol. Cell* **16**, 1673–1683 (2005).
46. J. H. Choi *et al.*, IgD class switching is initiated by microbiota and limited to mucosa-associated lymphoid tissue in mice. *Proc. Natl. Acad. Sci. U.S.A.* **114**, E1196–E1204 (2017).
47. P. Georgel, X. Du, K. Hoebe, B. Beutler, ENU mutagenesis in mice. *Methods Mol. Biol.* **415**, 1–16 (2008).
48. X. Zhong *et al.*, RNPS1 inhibits excessive tumor necrosis factor/tumor necrosis factor receptor signaling to support hematopoiesis in mice. *Proc. Natl. Acad. Sci. U.S.A.* **119**, e2200128119 (2022).
49. X. Zhong *et al.*, Genetic and structural studies of RABL3 reveal an essential role in lymphoid development and function. *Proc. Natl. Acad. Sci. U.S.A.* **117**, 8563–8572 (2020).
50. R. Song *et al.*, Trans-Golgi protein TVP23B regulates host–microbe interactions via Paneth cell homeostasis and Goblet cell glycosylation. *Nat. Commun.* **14**, 3652 (2023).
51. A. T. Kong, F. V. Leprevost, D. M. Avtonomov, D. Mellacheruvu, A. I. Nesvizhskii, MSFragger: Ultrafast and comprehensive peptide identification in mass spectrometry–based proteomics. *Nat. Methods* **14**, 513–520 (2017).
52. X. Zhong *et al.*, Essential requirement for IER3IP1 in B cell development. MassIVE. https://massive.ucsd.edu/ProteoSAFe/dataset.jsp?accession=MSV000091025. Deposited 9 January 2023.